Supporting Information

Ionogel-Perovskite Matrix Enabling Highly Efficient and Stable Flexible Solar Cells Towards Fully-R2R Fabrication

Yifei Kang, *Rong Li*, *Anran Wang*, *Jianye Kang*, *Zisheng Wang*, *Weihui Bi, Yang Yang*, *Yilong Song* and *Qingfeng Dong**

[1] State Key Laboratory of Supramolecular Structure and Materials, College of Chemistry, Jilin University, Changchun 130012, China

*Correspondence author. Email: *qfdong@jlu.edu.cn*

Experimental Procedures

Raw materials

Methylammonium iodide (MAI), lead iodide (PbI_2), C_{60}, bathocuproine (BCP), PEDOT:PSS were purchased from Xi'an Polymer Technology. 2,2,2-trifluoroethyl acrylate (>98.0%, TFOL-A, stabilized with MEHQ), 1-ethyl-3-methylimidazolium ethyl sulfate (>98.0%, $EMIMEtSO_4$) were purchased from TCI. 2-hydroxy-4'- (2-hydroxyethoxy) -2-methylpropiophenone (98%, UV2959) and acrylamide (98%, AAm) were purchased from energy chemical. Poly [bis(4-phenyl) (2,4,6-trimethylphenyl) amine] (average Mn 7000-10000, PTAA), choline chloride (≥99%) and all solvents were purchased from Sigma Aldrich.

Ionogel fabrication and characterization

The preparation method of IG is a modification based on previous work.[31] Firstly, AAm (690 mg) was dissolved in TFOL-A (1 mL) and $EMIMEtSO_4$ (3 mL) at 70 °C with vigorous stirring for about 30 min. After it was fully dispersed, UV2959 (9 mg) as initiator was added to the dispersion and transferred it to the glove box in order to exclude oxygen. Then, the dispersion was exposed to UV light (365 nm) for 30 min to finish the polymerization process and the final IG was obtained.

Mechanical tests were recorded by universal testing machine (instron 5944). The gauge length, width and thickness of the dumbbell-shaped samples in the tensile curve test were 8 mm, 1 mm, 1 mm, respectively. The adhesion area of ionogel to $MAPbI_3$ single crystal in tensile adhesion test was 3 mm^2. The cross-sectional length of the adhesion of ionogel to the grain boundary in shear adhesion test was 15 mm. The length, width and thickness of sample in resistance self-healing test were 3 cm, 2 mm, 1 mm, respectively.

Precursor solution fabrication

PVK precursor solution: 1.1 mmol $MAPbI_3$ was dissolved in 1 mL DMF.

IG-PVK precursor solution: 0.1wt% IG were dissolved in MA-based precursor solution to obtain different concentrations of IG-PVK solution.

Device fabrication

Solar cell devices fabrication: Flexible conductive substrate was cleaned by deionized water and ethanol, respectively, and then be treated with oxygen plasma for 15 min. The hole transport layer (HTL) was deposited on cleaned ITO by bar-coated PTAA (4 mg/mL in

toluene) at speed of 3 m/min along with air drying. For the perovskite layer, PVK or IG-PVK solution was coated using the same method on the HTL at speed of 2 m/min on the 65 °C substrate with a 60 μm gap. The resulting film was annealed for 10 min at 100 °C and the coating process mentioned above was fully completed in air without additional humidity control. Then, choline chloride was bar-coated on the perovskite film as passivation layer at a speed of 2.5 m/s at 50 °C with a 60 μm gap. Then, 25 nm C_{60}, 5.5 nm BCP and 80 nm Cu were sequentially deposited with the shadow mask by thermal evaporation under the pressure less than 5×10^{-4} Pa to complete the device fabrication.

SCLC device fabrication: flexible ITO/PTAA/perovskite/Au structured devices for space-charge-limited current (SCLC) measurement: perovskite films with or without IG were coated on PTAA modified ITO substrate, then 65 nm Au were deposited on perovskite films to complete the device fabrication.

Photovoltaic performance characterization

The photoelectric conversion performance of devices was measured under 1 Sun simulated AM 1.5G illumination by using an AAA class solar simulator of IEC 60904-9 Edition 2, ASTM E927-10 and JIS C8912 standards (SOLARBEAM-02-3A, CROWNTECH.INC.), with Keithley 2400 Source Measure Unit instrument. *J-V* curves were recorded in reverse and forward scan direction from -0.1 V to 1.2 V at the scan speed of 0.05 V/s. The active area was defined by a 0.0365 cm^2 shadow mask. The light intensity of 100 mW/cm^2 was calibrated by certified KG5 filtered standard Si solar cell. External quantum efficiency (EQE) spectra were measured by an CROWNTECH EQE measurement system using AC mode without extra light-soaking and bias processing.

Defect-related characterization

Detailed defect related characterization analyzation can be found in supplemental information.

Device stability test

Bending stability test: The device was placed on a programmable mechanical tester with adjustable bend radius and speed. Convex bends were employed to verify the tensile resistance properties of the IG-PVK film. For tension-only bending cycles, the bending radius was set at 5mm to prevent the ITO damage causing interference as shown in supplementary Video 2. Bending including ITO damage factor was also tested with a bending radius of 2.5 mm as shown in supplementary Video 3. Each bends cycle takes 2 s, no time interval between two cycles and there was no recovery time before testing the *J-V* curves unless specifically mentioned.

Continuous illumination operational stability test: perovskite devices with or without IG were measured following the ISOS-L-2I protocol at maximum power output point of device under modulated compound LED light source (100 mW/cm^2) that contained UV light and its spectrum is shown in Fig. S19. The unencapsulated devices were tested at ~65 °C in a N_2 chamber.[49]

Film characterization

X-ray diffraction spectra (XRD) measurement were performed by PANalytical B.V. Empyrean. SEM images were obtained by scanning electron microscope (HITACHI SU8000). In order to observe the morphology in the grain boundary in situ, the grain

boundaries were gradually broken under the bombardment of electron beams with an accelerating voltage of 10 KV and a beam current of 15 μA. Time-of-flight secondary ion mass spectrometry (TOF-SIMS) depth profiles was obtained by PHI nano TOF 2 with high mass resolution mode. The raster size is 100 μm×100 μm and sputtering was performed with pulsed Cs^+ and analysis was performed with a primary pulsed Bi^{3+} ion beam with an ion current of 2nA. The nano-IR spectroscopy was obtained by Nano IR 3 (Brucker). Photoluminescence (PL) and time-resolved PL spectra (TRPL) were carried out by Edinburgh Instrument FLS920. The XPS data was recorded by through X-ray photoelectron spectrometer (ESCALAB 250Xi). Raman spectra were measured by LabRAM HR Evolution (Horiba), excitation wavelength is 532nm. FTIR spectra were recorded by VERTEX 80V (Bruker). To observe the morphological changes of perovskite film under extreme tensile strain conditions, IG-PVK or PVK films were deposited on PDMS elastomer substrates coated with PEDOT:PSS (PH1000). After the annealing finished, they were stretched to 107% of their original length and fixed in that position, then we observed the morphology using SEM.

Defect-related characterization

Space-charge limited current (SCLC) method: The trap-filled limited voltages (V_{TFL}) of PVK and IG-PVK were acquired by measuring and fitting the corresponding dark-state *J-V* curves of ITO/PTAA/perovskite/Au structured hole-only device, and the V_{TFL} was calculated by the below Formula:[42]

$$V_{TFL} = \frac{enL^2}{2\varepsilon\varepsilon_0}$$

Where

e is the electron charge;

n is the density of trap states;

L is the thickness of the film;

ε is the relative dielectric constant.

ε_0 is the vacuum dielectric constant (8.84×10^{-14} F/cm^2);

Thermal admittance spectroscopy (TAS) method: To compare the energy profile of trap-states in PSCs with and without IGs before and after bending, we tested the C-f curves of IG-PVK and PVK devices using Agilent E4980A with 20 mV AC voltage level and no DC bias. The scanning frequency range of the AC voltage is from 0.1 KHz to 2000 KHz. Using the frequency-dependent capacitance, the energy-dependent trap density of states (tDOS) can be derived using the following equation:[43]

$$N_t(E_f) = -\frac{V_{bi} dC \ f}{eWdfk_BT}$$

where

N_t is the tDOS;

E_f is the energetic demarcation corresponding to each frequency;

V_{bi} is the built-in potential, which was derived from the Mott–Schottky analysis;

C is the capacitance corresponding to each frequency;

W represents depletion width, assuming that the perovskite layer is completely depleted, so its value is approximately equal to the thickness of the perovskite layer.

f is the frequency;

k_B is the Boltzmann's constant;

T is the thermodynamic temperature.

The E_f is defined by using angular frequency $E_f = k_B T ln(\frac{\omega_0}{2\pi f})$, where ω_0 is the attempt to escape angular frequency which was ~1.0 × 10^{12} Hz for $MAPbI_3$. That was calculated by $2\pi v_0 T^2$ (v_0 is the temperature-dependent attempt to escape frequency extracted from the temperature-dependent C-f measurements by fitting $ln\frac{T^2}{2\pi f}\frac{1}{T}$ to obtain the intercept which equal to $\ln(2\pi v_0)$).

Capacitance-Voltage (C-V) method: C-V method is a simple and common method to directly characterize the spatial distribution of charge density N_c, which contains the response of bulk, interface trap density and free charge density. We apply the depletion layer capacitance theory to PSCs by changing the depletion layer width by inputting different DC voltages, then read the capacitance values at each voltage to calculate the corresponding charge density (N_c) for each edge of depletion layers. The DC bias ranged from 0 to 1.2 V, A small AC bias perturbation is employed with the frequency and amplitude remain unchanged at 10 kHz and 20 meV, respectively.

The N_c at each edge of the depletion region can be calculated from the following equation:[44]

$$N_c(X) = -\frac{2}{e\varepsilon\varepsilon_0 A^2}\left[\frac{d(1/C^2)}{dV}\right]^{-1}$$

where X is the profiling distance from the junction barrier. It can be derived from: $\frac{X}{W} = \frac{C_g}{C}$, where C_g can be considered as the geometric capacitance at zero DC bias, C is the specific capacitance;

V is the corresponding voltage;

A is the area of the device.

Assuming that the free charge density of the device is almost unchanged before and after bending, the increased charge density is mainly provided by the bulk and interface trap density. Based on this theory, the spatial distribution of the increased defect density of IG-PVK and PVK before and after bending can be obtained.

Supplementary Text

Supplementary Discussion: the reason for the improved bending stability of IG-based flexible devices under small radius bending.

On the one hand, as shown in the Fig. S17, dense macroscopic cracks were observed for PVK film under small radius bends, which would cause a significant increase in leakage current. In addition, friction between crystal grains during bending would generate new defect sites (Fig. 3H-I). Besides, the cracks of ITO may also extend to the control perovskite layer and cause further damage to the surface. These factors lead to a significant drop in J_{SC}, V_{OC}, and FF of control device (Fig. S16).

On the other hand, due to the dissipation of grain boundary stress and healing of the

defects by IG, it can effectively attenuate the effect of destroyed ITO on the morphology of the upper perovskite film. In addition, the cladding of grain boundaries by IG also effectively prevented new defect sites generated by grain friction. Therefore, the efficiency loss of the bent IG-PVK device mainly came from the decrease of FF caused by the increase of series resistance.

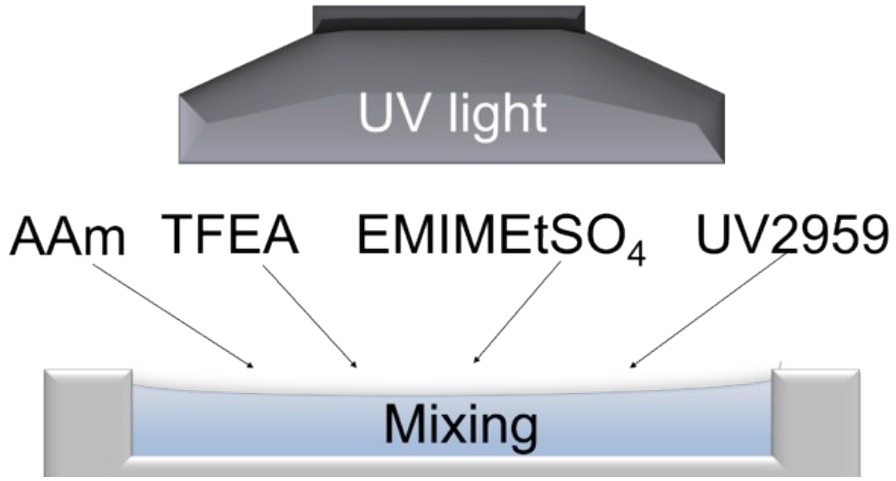

Figure. S1: Schematic diagram of the ionogel synthesis process.

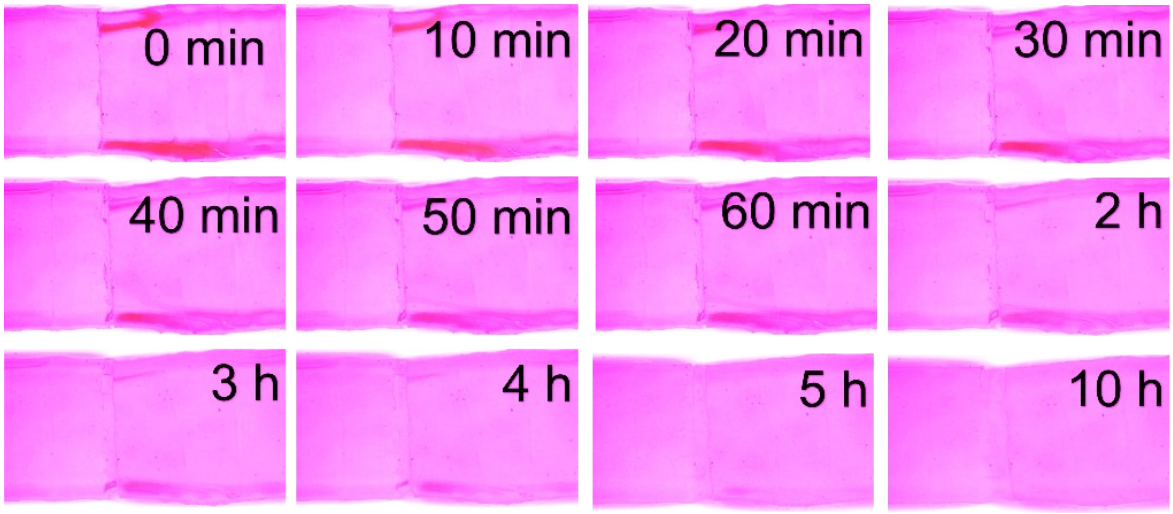

Figure. S2: In situ observation of time-resolved recoupling of cut ionogel by self-healing process.

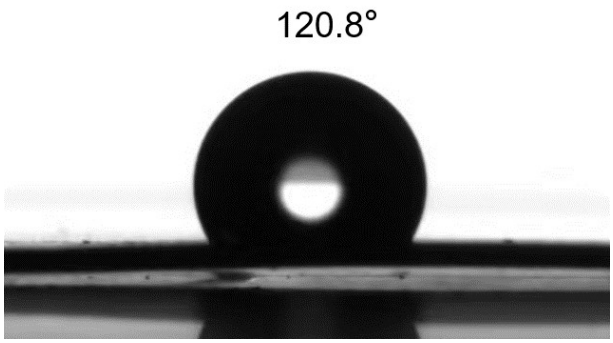

Figure S3: Water contact angle of the PTFE substrate.

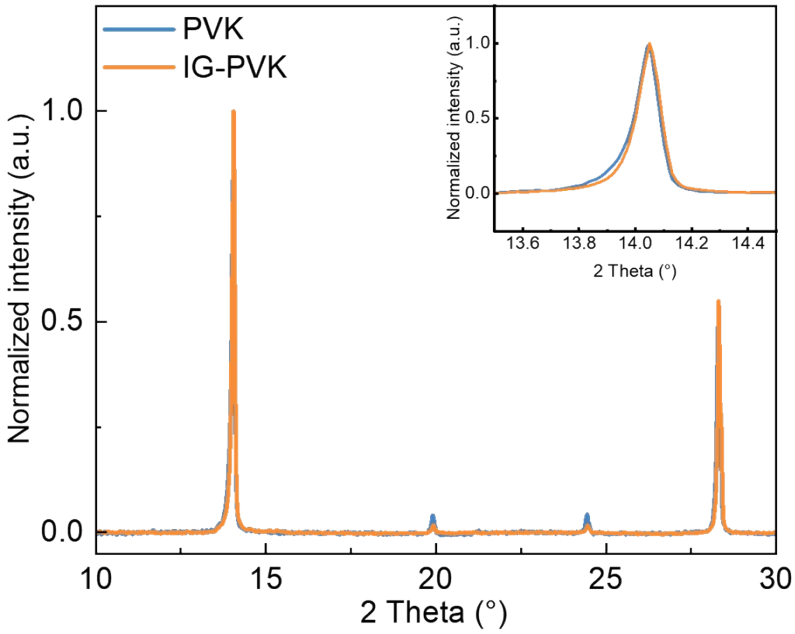

Figure S4: Comparison of XRD pattern of IG-PVK and PVK films.

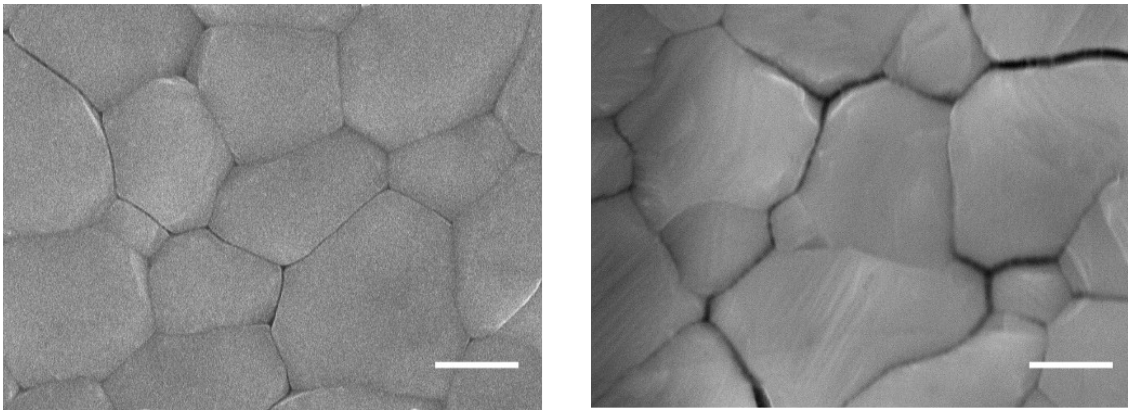

Figure. S5: SEM images of IG-PVK (left) and PVK (right) films. Scale bar: 500 nm.

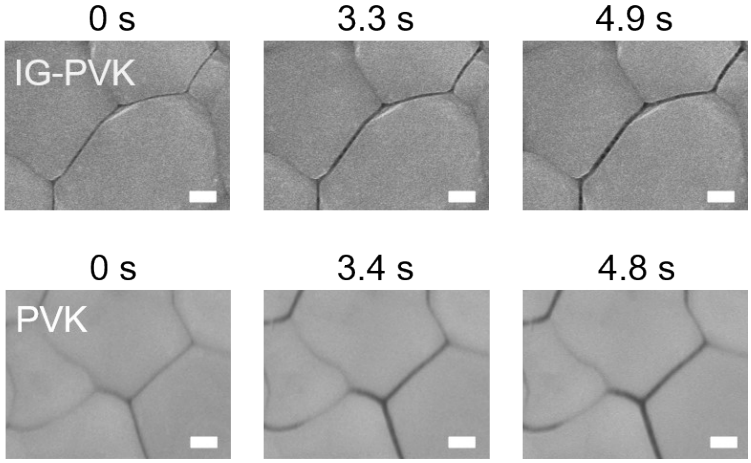

Figure. S6: Time-dependent morphology of IG-PVK (above) and PVK (below) film under intense electron beam bombardment. Scale bar: 200 nm.

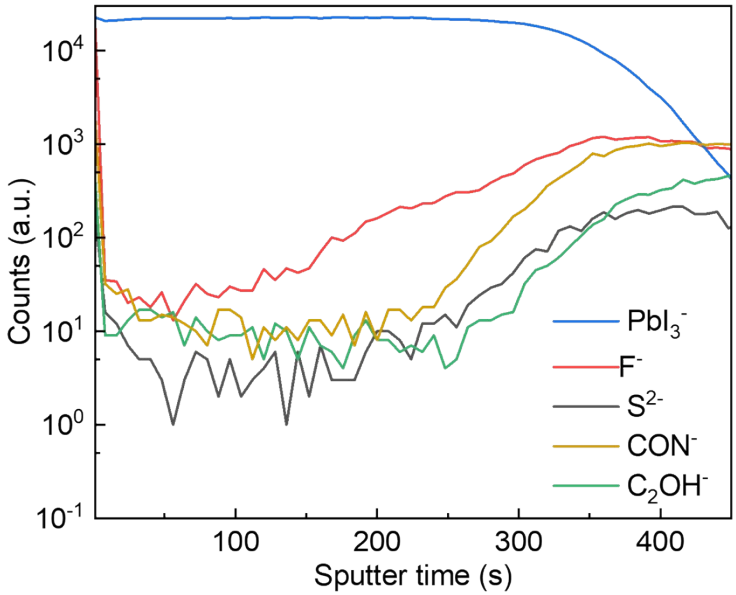

Figure S7: TOF-SIMS spectra of IG-PVK film.

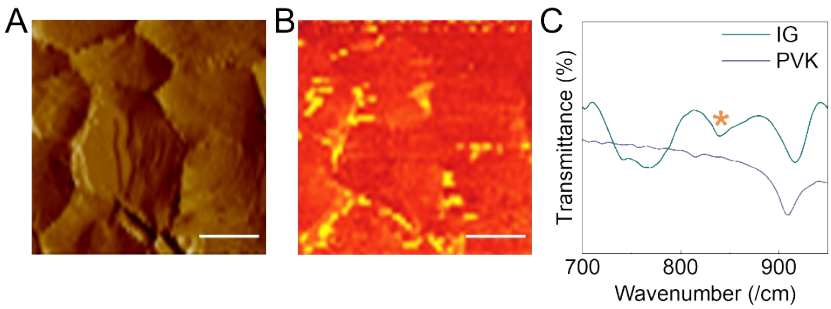

Figure S8: (A-B) AFM phase images (A) and the corresponding nano-IR spectra mapping (B) of IG-PVK film. Scale bar: 500 nm. (C) Comparison of Fourier Transform Infrared (FTIR) spectra between IG and PVK powder, 842 cm^{-1} was chosen as a characteristic peak to probe the distribution of ionogel near the surface.

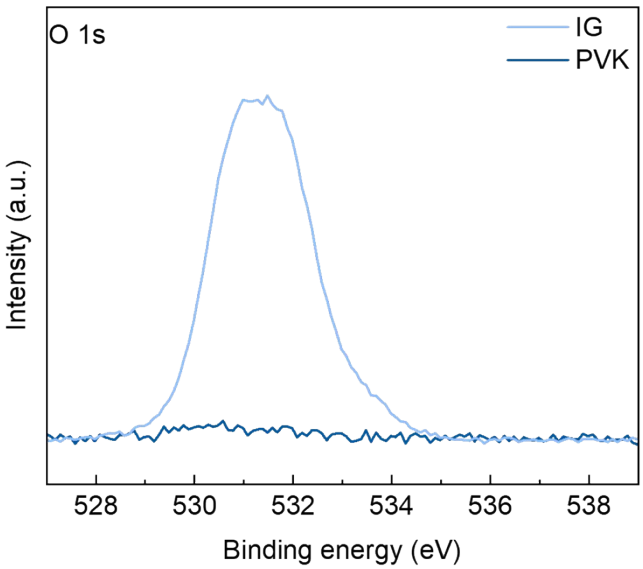

Figure S9: Comparison of O 1s peak of IG and PVK films from XPS results. the results showed that the signal of O in PVK sample was very weak and almost undetectable, which eliminated the possibility of surface contamination.

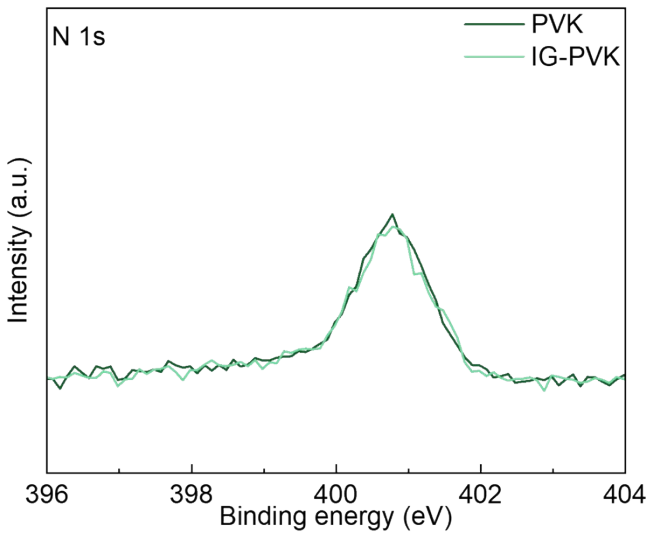

Figure S10: Comparison of N 1s peak of IG-PVK and PVK films from XPS results. The peak of N is a single peak, which eliminated the possibility of surface degradation.

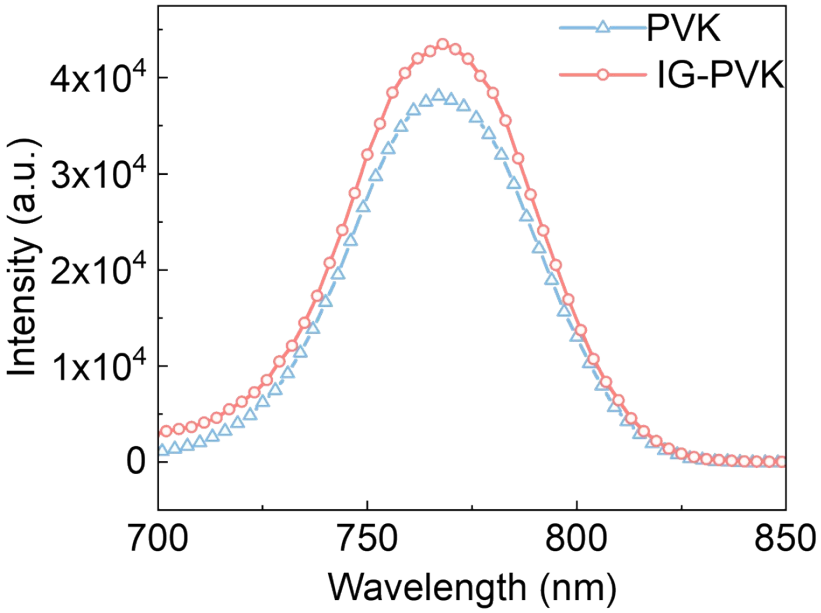

Figure. S11: Photoluminescence spectra of IG-PVK and PVK films.

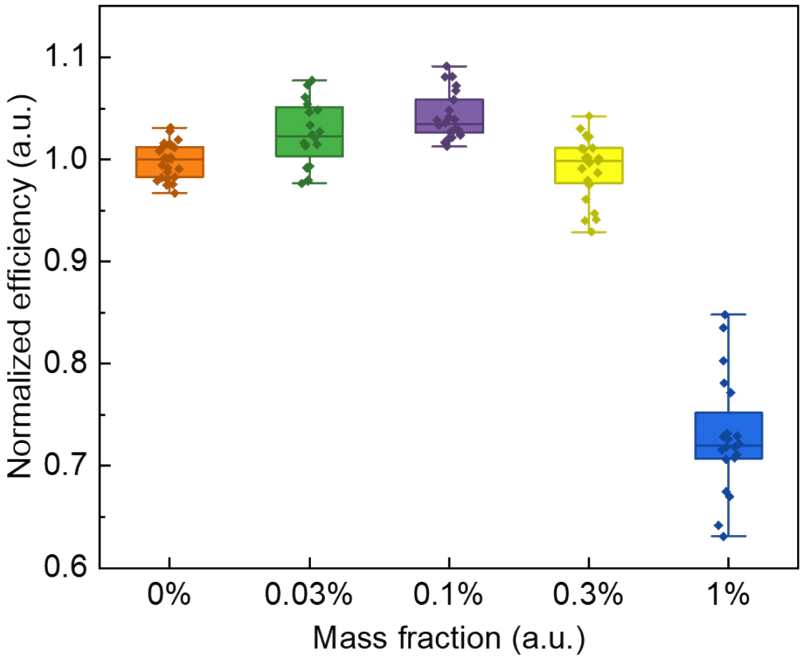

Figure. S12: Statistic distribution of normalized devices efficiency doped with different concentrations of IG.

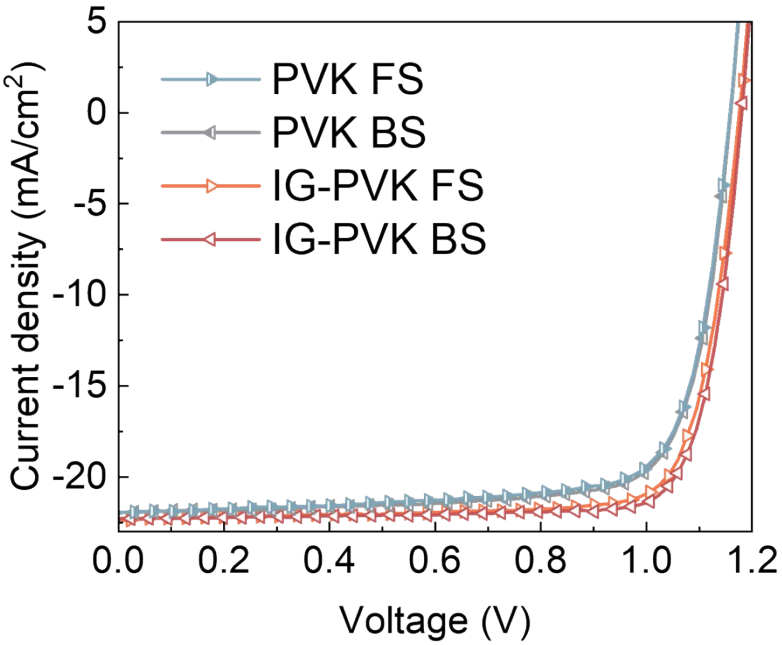

Figure. S13: *J-V* curves of IG-PVK and PVK devices obtained by forward scanning or backward scanning.

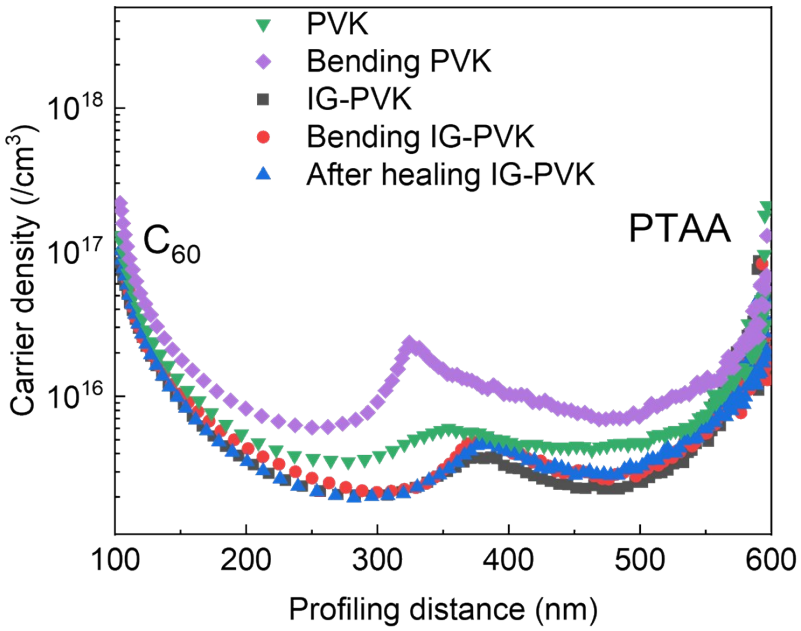

Figure. S14: Profiling distance-dependent carrier density of IG-PVK and PVK flexible devices before and after bending.

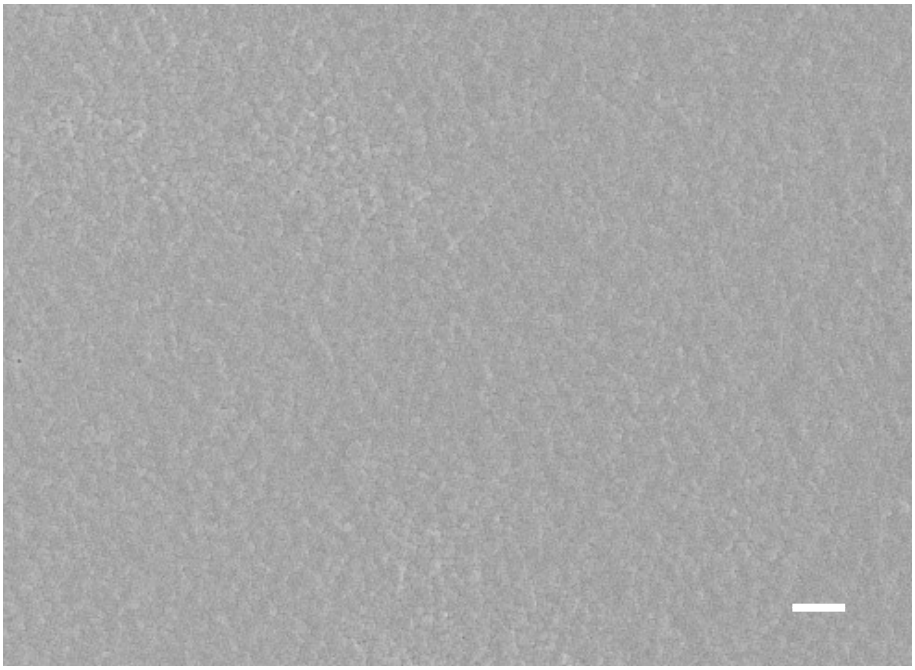

Figure. S15: SEM images of damaged IG-PVK films after self-healing for 10 h. Scale bar: 5 μm.

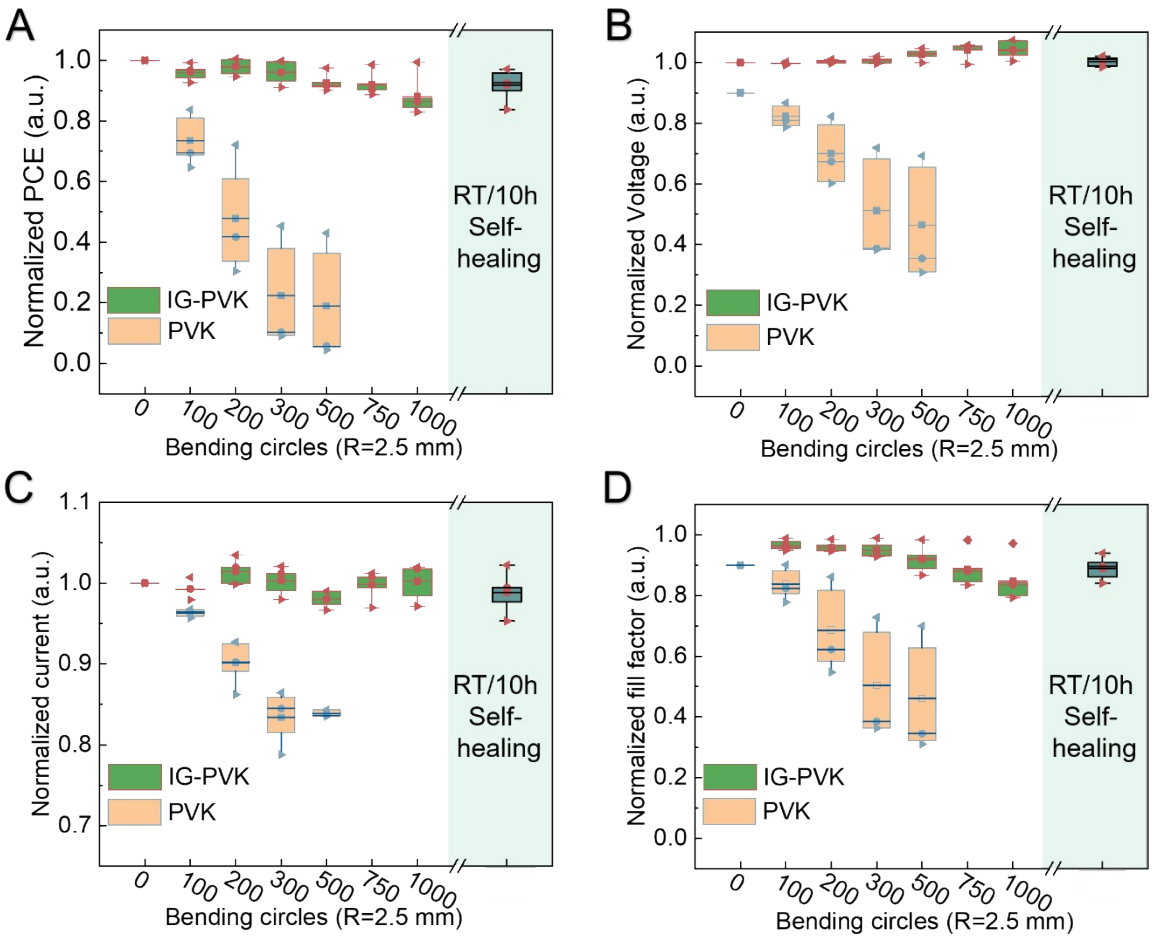

Figure. S16: Bending-dependent efficiency (A), open circuit voltage (B), short circuit current density (C), fill factor (D) distribution curves of IG-PVK and PVK devices under 2.5 mm convex bending radius. The shaded areas showed the performance parameters distribution of the bent IG-PVK devices after room temperature self-healing process for 10 h. ❖ represented the maximum value, ◆ represented the minimum value, ☐ represented the main value, represented the median value, and the box covered the area between the 25th percentile and the 75th percentile.

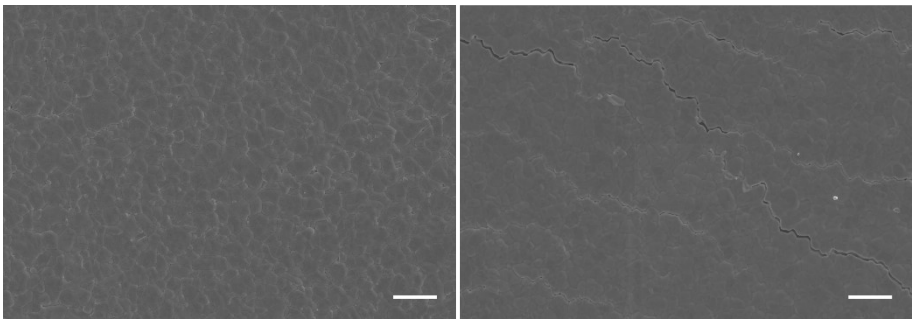

Figure S17: Comparison of IG-PVK (left) and PVK (right) devices morphology after bending under 2.5 mm radius. Scale bar: 5 µm.

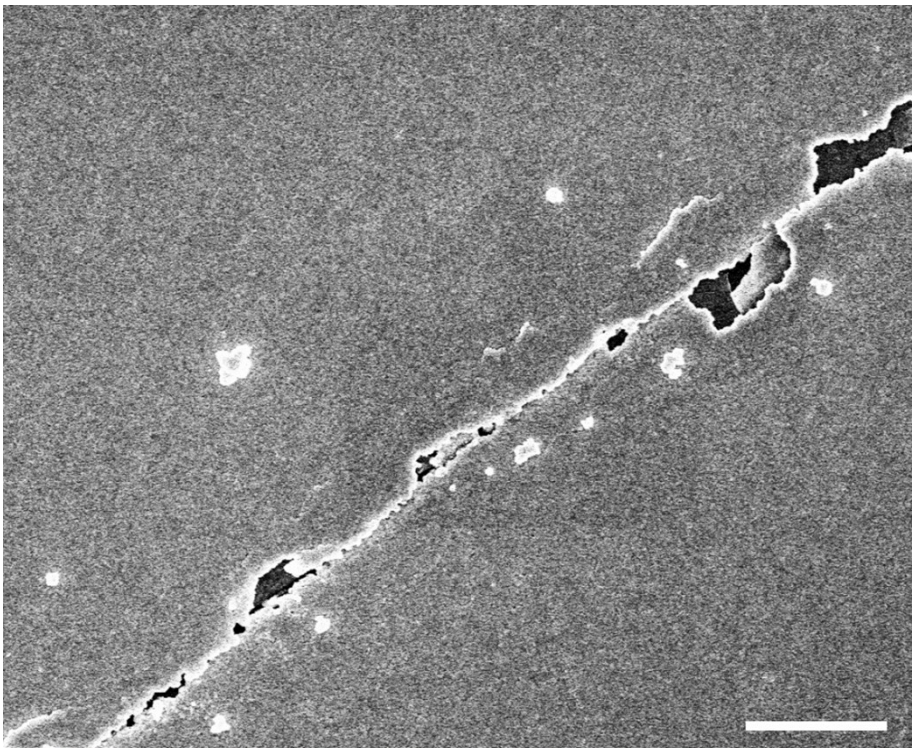

Figure. S18: SEM images of interlayer debonding of stretched PVK films after releasing the stress on Polydimethylsiloxane (PDMS) substrate. Scale bar: 10 μm.

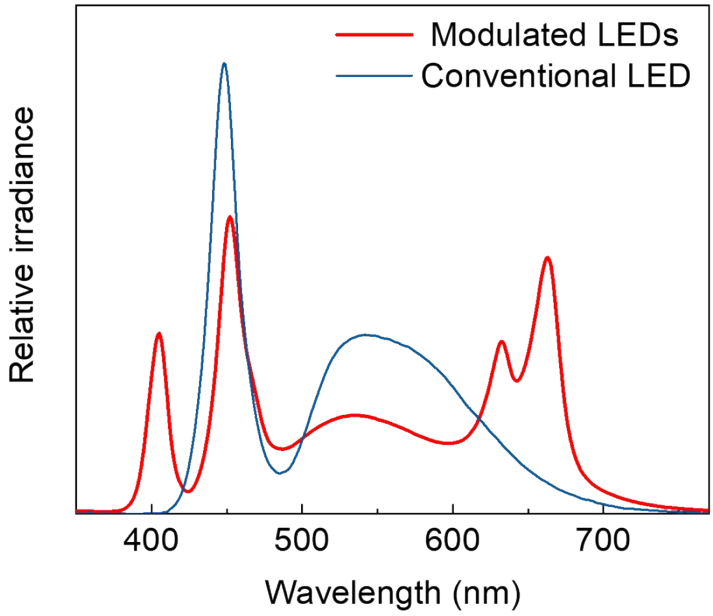

Figure. S19: Spectra of light sources used for operational stability and conventional LED light sources.

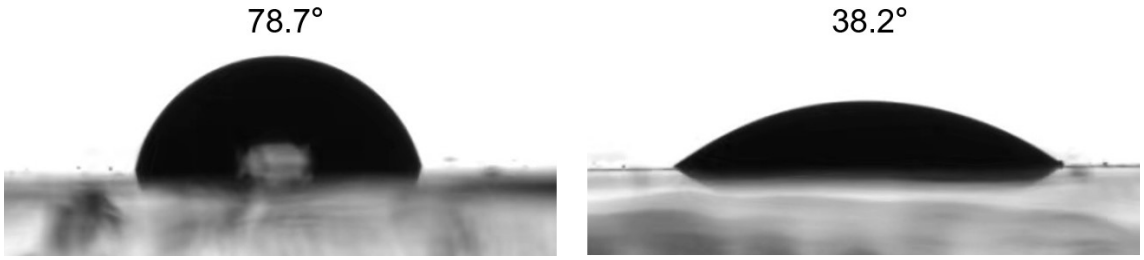

Figure S20: Water contact angle of the perovskite film before (38.2°) and after (78.7°) adding IG.

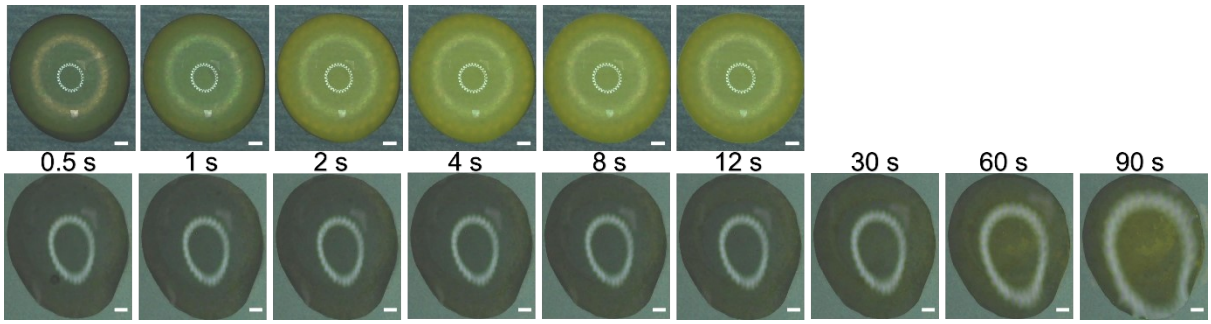

Figure. S21: The whole time-resolved topography of IG-PVK (bottom) and PVK (top) films after water droplets dropped on the film surface. Scale bar: 100 μm.

Device Structures	Best PCE (%)	SPO (%)	FF (%)	*V*oc loss (V)	Fabrication Method	Fabrication Environment	Operational Stability*	Mechanical stability			Ref.
								bending radius (mm)	bending circles	Retained PCE(%)	
n-i-p	20.40	20.03	80.67	~0.410	spin coating	glove box	\	10	2000	90.6	[52]
p-i-n	20.50	\	81.22	~0.433	spin coating	glove box	\	2.5	10000	88	27
n-i-p	20.7	\	79.5	~0.331	spin coating	glove box	T_{80}~120 h	10	1000	~85	[53]
n-i-p	21.0	20.6	77.9	~0.400	spin coating	glove box	T_{90}~800 h	5	10000	88	1
n-i-p	21.10	20.3	80.35	~0.404	spin coating	glove box	3 h with no attenuation	10	2000	93.2	[54]
n-i-p	21.11	20.3	78.9	~0.386	spin coating	glove box	\	8	3000	~90	[55]
n-i-p	21.63	20.55	78.3	~0.407	spin coating	\	$T_{98.8}$~48 h	5	10000	91.8	[56]
p-i-n	21.73	21.44	77.68	~0.393	spin coating	glove box	$T_{89.56}$~1000 h	5	1000	94-98	2
n-i-p	22.37	21.79	82.89	~0.363	spin coating	glove box	$T_{94.5}$~110 h	7	4000	90	4
n-i-p	22.44	\	78.16	~0.351	spin coating	\	\	5	1000	~90	5

Device Structures	Best PCE (%)	SPO (%)	FF (%)	*V*oc loss (V)	Fabrication Method	Fabrication Environment	Operational Stability*	Mechanical stability			Ref.
								bending radius (mm)	bending circles	retained PCE (%)	
p-i-n	18.12	18.01	74.44	~0.423	meniscus coating	air (RH 10%-20%)	\	4	4000	~80	[37]
n-i-p	19.1	18.8	75.5	~0.395	gravure-printed	\	\	\	\	\	3
p-i-n	19.15	19.11	78.65	~0.468	meniscus coating	\	600 h with no attenuation	4	5000	~87	28
p-i-n	19.41	19.05	81	~0.468	blade coating	Glove box	\	3	2000	80	9
p-i-n	19.7	19.5	80	~0.474	blade coating	\	T_{88}~1000 h	3	5000	85	[38]
p-i-n	19.87	19.52	79	~0.389	meniscus coating	Glove box	\	3	7000	85	[39]
p-i-n	20.16	\	80.19	~0.454	blade coating	Glove box	\	3	2000	55	[41]
p-i-n	20.56	20.11	78.3	~0.450	meniscus coating	\	T_{98}~200 h	3	10000	~80	[40]
p-i-n	**21.76**	**21.7**	**82.33**	**~0.367**	**blade coating**	**air**	**T_{90}~1336 h**	**5**	**25000**	**~90**	***This work***

SPO stands for stabilized power output efficiency.

Table. S1: Statistics of the reported performance parameters of flexible devices based on spin-coating and large-area coating process.